

Unleashing Quantum Simulation Advantages: Hamiltonian Subspace Encoding for Resource Efficient Quantum Simulations

M. H. Cheng,^{1,2,*} Yu-Cheng Chen,^{3,4,*} Qian Wang,³ V. Bartsch,² M. S. Kim,^{1,†} Alice Hu,^{3,5,‡} and Min-Hsiu Hsieh^{4,§}

¹*Department of Physics Blackett Laboratory, Imperial College London, SW7 2AZ, United Kingdom*

²*Fraunhofer Institute for Industrial Mathematics,
Fraunhofer-Platz 1, 67663 Kaiserslautern, Germany*

³*Department of Mechanical Engineering, City University of Hong Kong, Kowloon, Hong Kong SAR 999077, China*

⁴*Hon Hai (Foxconn) Research Institute, Taipei, Taiwan*

⁵*Department of Materials Science and Engineering,
City University of Hong Kong, Kowloon, Hong Kong SAR 999077, China*

Number-conserved subspace encoding for fermionic Hamiltonians, which exponentially reduces qubit cost, is necessary for quantum advantages in variational quantum eigensolver (VQE). However, optimizing the trade-off between qubit compression and increased measurement cost poses a challenge. By employing the Gilbert-Varshamov bound on linear code, we optimize qubit scaling $O(N \log_2 M)$ and measurement cost $O(M^4)$ for M modes N electrons chemistry problems. The compression is implemented with the Randomized Linear Encoding (RLE) algorithm on VQE for H_2 and LiH in the 6-31G* and STO-3G/6-31G* basis respectively. The resulting subspace circuit expressivity and trainability are enhanced with less circuit depth and higher noise tolerance.

Introduction.—Simulating many-body fermionic systems is essential for fields like quantum chemistry, condensed matter, and high energy physics [1–3]. It promises better designs for batteries and drugs, new quantum technologies, and discovering the exotic nature of reality [4–6]. However, accurate classical fermionic simulation requires exponential computational resources [7]. While a quantum computer is expected to overcome this limit, it remains a central challenge to demonstrate quantum advantages in this domain.

Electronic structure Hamiltonian encoding maps fermionic operators from the Fock space to qubit operators in the qubit space. The standard approaches such as the Jordan-Wigner, Parity, and Bravyi-Kitaev transformation [8, 14] encode M fermionic modes to M qubits, regardless of the number of electrons N . However, since all fermionic Hamiltonians must conserve fermions, interesting physics depends only on the particle conserved subspace, which takes only $[N \log M]$ qubits to encode in the precision limit $M \gg N$ [15, 16]. Logarithmic scaling in M is necessary for simulating high precision limit, which demands an enormous basis set. Subspace encoding provides an exponential improvement in encoding quantum chemistry problems, a step that can potentially advance near-term electronic structure simulation with the Noisy Intermediate Scale Quantum (NISQ) devices [17].

Another important but often overlooked aspect of fermionic Hamiltonian encoding is the measurement cost required to infer the two-electron reduced density matrix (2-RDM) – the quantum chemistry observable that deter-

mines properties of the electronic properties. Unlike classical molecular simulation, quantum encoding would affect the measurement complexity. Efficient 2-RDM measurement cost is necessary for achieving large-scale quantum simulation. For example, the Qubit Efficient Encoding (QEE) [12] has attained the $[N \log_2 M]$ qubit scaling via a direct fermionic state to qubit state encoding, but plagues with inexact fermionic gate implementation and unscalable measurement cost of $O(M^N)$. It limits its applications to fermionic systems with few electrons.

The middle ground leveraging between qubit reductions and measurement cost is linear compression. Unlike QEE, all linear compression exhibits near optimal measurement cost concerning M , and allows for implementation of single and double excitations without approximation. Linear compression method such as the segment code [9] and graph-based encoding [10] achieves $O(M/N)$ qubit reduction, whose compression rate unfortunately, drops significantly as N increases. The best linear encoding has poly-logarithmic $O(N^2(\log_2 M)^4)$ qubit scaling [11], which is too large for any near-term, or even for long-term applications. The optimal compression rate has remained unknown.

Observing the correspondence between linear compression and its dual code [10], it turns out that we can reformulate fermionic encoding in the language of classical error correction code. In this letter, we study optimal linear encoding utilizing dual code correspondence. We reformulate a linear compression in terms of its dual code, the parity check matrix. Linear compression under the particle-conserved symmetry can be translated into finding a classical error-correcting code with minimal redundancy, given a fixed code distance. The correspondence maps the conserved particle number N to the code distance $2N + 2$. Via applying the Gilbert-Varshamov (GV) bound [18, 19] on the dual code, we prove that optimal linear compression has qubit resource upper bound

* These authors contributed equally to this work

† m.kim@imperial.ac.uk

‡ alicehu@cityu.edu.hk

§ min-hsiu.hsieh@foxconn.com

	Jordan Wigner [8]	Segment [9]	Graph-Based [10]	Polylog [11]	QEE [12]	Our Work
Qubit cost	$O(M)$	$O(M)$	$O(M)$	$O(N^2(\log M)^4)$	$O(N \log M)$	$O(N \log M)$
Measurements	$O(M^3)$ [13]	$O(M^4)$	$O(M^4)$	$O(M^4)$	$O(M^N)$	$O(M^4)$

TABLE I. Table for the comparison of previous linear and non-linear encoding scheme with our RLE schemes at the asymptotic regime $M \gg N$.

$2N \log_2 M$. With an optimal linear encoder, we propose a framework that connects binary vector space transformation with qubit operator transformation. Under this framework, we show the measurement cost of the 2-RDM is at most $1 + \binom{M}{2} + \binom{M}{4}$, and untrotterized implementation of the first and second excitation gates. In Table I, our result shows the best qubit to measurement trade-off compared to previous encodings. Finally, we propose the Randomized Linear Encoding (RLE) algorithm, which employs a randomized sampling technique for finding the optimal compression. Numerical study shows that it solves for encoding which obeys the $2N \log_2 M$ bound. We compare our algorithm to the segment code and graph-based encoding and realize that our qubit compression rate surpasses theirs for all N and M . For example, we can encode a 2 electron problem with 580 fermionic modes within 30 qubits; unlike previous ab initio methods which can at max encode 59 modes with the same electron number and qubit resources [10].

We test the ground state accuracy of H_2 and LiH system before and after compression with variational quantum eigensolver (VQE) [20] with the hardware efficient ansatz (HEA) [21, 22]. With RLE, H_2 molecule simulation in 6-31G basis demonstrates a 5 qubits reduction and achieves chemical accuracy across all bond lengths. LiH in STO-3G basis achieves substantial circuit depth reduction for state preparation, 4 orders of magnitude higher energy precision, and is more robust against the noise of the quantum computer. LiH in 63-1G* demonstrates 8 qubits reductions and chemical accuracy, compared to the uncompressed case that does not converge even in the noiseless simulator. In general, the compressed Hilbert space can generate more physical state expressive and trainable ansatz, higher resistance to noise, and substantially less gate cost for state preparation. Logarithmic scaling in the qubit resource, combined with polynomial scaling in the measurement cost, promises unparalleled advantages for fermionic simulation with variational quantum algorithms. We expect our work to find applications to VQE problems for large molecular systems.

General Framework—Given a second-quantized electronic structure Hamiltonian of the form,

$$\hat{H} = \sum_{ij} h_{ij} \hat{a}_i^\dagger \hat{a}_j + \sum_{ijkl} g_{ijkl} \hat{a}_i^\dagger \hat{a}_j^\dagger \hat{a}_k \hat{a}_l, \quad (1)$$

we can encode first and second excitation operators $\hat{a}_i^\dagger \hat{a}_j$ and $\hat{a}_i^\dagger \hat{a}_j^\dagger \hat{a}_k \hat{a}_l$, which we collectively denote them as \hat{O} , to qubit operators via different linear encoding schemes, such as the commonly used JW transformation [23]. However, the existing methods have not demonstrated a

complete use of particle-conserved subspace, and neither has the literature fully explored the explicit relationship between linear encoder and qubit operator encoding.

We establish the relationship with the following formalism. Each excitation operator \hat{O} can be associated with binary vectors $\vec{a}, \vec{b}, \vec{c} \in \mathbb{F}_2^M$. Specifically, \vec{c} encodes the parity information of \vec{b} , and \vec{a} induces the transitions $\vec{b} \rightarrow \vec{a} \oplus \vec{b}$ on $\vec{b} \in S_{\hat{O}}$, where $S_{\hat{O}}$ is the set of states in the number-conserved subspace on which the operator \hat{O} acts and this set is unique to each first and second excitations.

In our framework, the (anti-)Hermitian component of \hat{O} can be decomposed into X-string $X^{\vec{a}}$, sign information $(-1)^{\vec{c} \cdot \vec{b}}$ and a set of P-strings $P^{\vec{b}} \pm P^{\vec{a} \oplus \vec{b}}$:

$$\text{Re/Im}\{\hat{O}\} = X^{\vec{a}} \sum_{\vec{b} \in S_{\hat{O}}} (-1)^{\vec{c} \cdot \vec{b}} (P^{\vec{b}} \pm P^{\vec{a} \oplus \vec{b}}). \quad (2)$$

This framework generalises the decomposition technique in Ref~[10] and the use of projectors in Ref~[12]. The sign function $(-1)^{\vec{c} \cdot \vec{b}}$ is a consequence of absorbing Pauli-Z strings, which encodes the parity operator, represented in terms of the Z-strings, of \hat{O} into the P-strings:

$$Z^{\vec{c}} P^{\vec{b}} = (-1)^{\vec{c} \cdot \vec{b}} P^{\vec{b}}. \quad (3)$$

We define X-string, Z-string, and P-strings as follows:

$$X^{\vec{b}} = \prod_{m=1}^M X_m^{\vec{b}[m]}, Z^{\vec{b}} = \prod_{m=1}^M Z_m^{\vec{b}[m]}, P^{\vec{b}} = \prod_{m=1}^M P_m^{\vec{b}[m]} \quad (4)$$

with $\vec{b}[m]$ denotes the m th entry of the vector, $X/Z_i = \hat{\sigma}_{x/z,i}$, and $P^0 = \frac{1+Z}{2}$, $P^1 = \frac{1-Z}{2}$. binary vector space \mathbb{F}_2^M is thus reflected on the exponent of the operator. Transformation on the vector space can be directly mapped to operator transformation. Provided with a $M \times M$ binary matrix \mathbf{G} , we can show that the operators transforms as [9]:

$$X^{\vec{b}} \rightarrow X^{\mathbf{G}\vec{b}}, Z^{\vec{b}} \rightarrow Z^{(\mathbf{G}^{-1})^T \vec{b}}, P^{\vec{b}} \rightarrow P^{\mathbf{G}\vec{b}} \quad (5)$$

We can directly apply JW, Parity, and BK encoding matrices, defined in Ref~[14], on Eqn~5 for qubit operator encoding.

Meanwhile, when the matrix becomes a subspace projection, the transformation of $Z^{\vec{b}}$ breaks down due to a lack of left inverse, affecting the measurement complexity. By replacing the Z-strings with the P-strings, we can avoid compressing with the Z-string. Suppose now \mathbf{G} is

a $Q \times M$ linear encoder, the qubit operators can simply be encoded as:

$$\text{Re/Im}\{\mathcal{E}(\hat{O})\} = X^{\mathbf{G}\tilde{\mathbf{a}}} \sum_{\tilde{\mathbf{b}} \in S_{\hat{O}}} (-1)^{\tilde{\mathbf{c}} \cdot \tilde{\mathbf{b}}} (P^{\mathbf{G}\tilde{\mathbf{b}}} \pm P^{\mathbf{G}(\tilde{\mathbf{a}} \oplus \tilde{\mathbf{b}})}) \quad (6)$$

where $\mathcal{E}(\cdot)$ denotes the encoding map for the qubit operator \hat{O} . Qubit operator linear encoding reduces to seeking for the optimal linear encoder \mathbf{G} .

To study symmetry constraint on \mathbf{G} , we explore the optimal scaling of \mathbf{G} in the perspective of dual code. For every $Q \times M$ linear compression \mathbf{G} , we can construct its $(M - Q) \times M$ dual code \mathbf{P} such that $\mathbf{G}\mathbf{P}^T = 0$. In the dual code formalism, solving for a qubit minimized encoder \mathbf{G} is equivalent to seeking a maximal dimension of \mathbf{P} . $\mathbf{G}\mathbf{P}^T = 0$ implies that \mathbf{P} generates equivalent classes on the unencoded space for each binary vector $\tilde{\mathbf{b}}$:

$$\tilde{\mathbf{b}} \sim \tilde{\mathbf{b}} \oplus \mathbf{P}^T \tilde{\mathbf{e}} \quad (7)$$

for any $\tilde{\mathbf{e}} \in \mathbb{F}_2^{M-Q}$. The conserved quantity N – the number of fermions in the system – dictates that each Hamming weight N unencoded codeword shall appear in each equivalent class only once. Since only the even Hamming weight elements in \mathbf{P}^T can subjectively encode the number-conserved vectors, the conserved quantity N places a lower bound to the code distance $2N + 2$ of the even sub-code of the dual code \mathbf{P} . Thus, given a fixed code distance $2N + 2$, and the size of the dual code M , we can apply the Gilbert-Varshamov bound on the even subspace of \mathbf{P} , which constrains the maximal dimension of $M - Q$ as follow:

Theorem 1. *The minimal qubit cost required to encode a M fermionic modes N electrons problem has the upper bound of $Q \leq 2N \log M$.*

Proof. See Appendix C. \square

This result shows that linear compression can significantly reduce the cost of hardware for implementing VQE. Unlike first-quantized encoding, this holds true for any choice of basis set and doesn't require antisymmetrization [24, 25]. Additionally, rather than directly building a linear encoder, we can borrow techniques for constructing classical error correction codes, which are already established, to create the parity check matrix.

Now we investigate the impact of linear encoder on the property of qubit operator. Due to the broken transformation on the Z-string, it is necessary to express the qubit operator in the encoded space only in terms of X-string and P-string. While this would increase the Pauli terms in expressing qubit operators in Eqn~(6), we can in fact show that those Pauli terms must be mutually commuting, and that leads to our second result:

Theorem 2. *The cost of measurement basis of a linearly encoded quantum chemistry Hamiltonian is upper bounded by $1 + \binom{M}{2} + \binom{M}{4}$.*

Proof. See Appendix D. \square

For linear encoding, we have shown that for each set of fermionic modes i, j, k, l , it takes only one basis to measure the 2-RDM observables $\text{Re/Im}\{\hat{a}_i^\dagger \hat{a}_j^\dagger \hat{a}_k \hat{a}_l\}$. In other words, linear encoding does not increase the complexity of calculating RDM elements. An often overlooked aspect of quantum advantage is the scaling of the measurement scaling. We note that measurement scaling is *in fact* a part of the computational complexity. If measurement scalability is lost in an encoding, such as the QEE method, there is no quantum advantage in calculating observable quantities compared to classical methods. The same result is also important for implementing fermionic gates in the electronic structure Hamiltonian. Since the encoded Pauli elements of each \hat{O} must be mutually commuting, linear encoding allows *exact* fermionic gate implementation such as the first and second excitations. Compared to QEE, implementing the same gate would require Trotterisation due to the presence of non-commuting terms, which would significantly increase the gate complexity.

In comparison, the JW representation has the extra property that we can simultaneously measure $\text{Re/Im}\{\hat{a}_i^\dagger \hat{a}_j^\dagger \hat{a}_k \hat{a}_l\}$ and $\text{Re/Im}\{\hat{a}_m^\dagger \hat{a}_n^\dagger \hat{a}_o \hat{a}_p\}$ provided that $i, j, k, l \neq m, n, o, p$. Thus, measurement cost of the observable $\text{Re/Im}\{\hat{a}_i^\dagger \hat{a}_j^\dagger \hat{a}_k \hat{a}_l\}$ in the JW representation is $\mathcal{O}(M^3)$ [13]. For NISQ and fault tolerant devices, a polynomial trade-off in measurement for an exponential qubit cost improvement would be desirable. Meanwhile, unlike first-quantized encoding where we need to worry about the scaling of Pauli terms [26], the measurement cost in the second quantized linear encoder does not depend explicitly on the Paulis scaling. Linear encodings provide a natural grouping of the Paulis. Provided that the second electronic integral g_{ijkl} is sparse, we expect that the actual measurement cost would be much less than the bound $1 + \binom{M}{2} + \binom{M}{4}$.

While we have analytically shown the theoretical upper bound of optimal fermionic linear compression, the next question is whether we can generate optimal linear encoding. That leads to our algorithm.

Randomized Linear Encoding—Since the current deterministic linear encoding methods [9, 11] are far from the theoretical bounds, we propose the Randomized Linear Encoding algorithm (RLE), which employs a randomized search technique to converge the linear encoder to the $2N \log_2 M$ upper bound.

RLE begins its random search by choosing a Q within the bounded region $N \log_2 M < Q < 2N \log_2 M$. Upon selecting the qubit size, RLE initializes the generator matrix $\mathbf{G} = [I_Q | D]$ in the *standard basis* [27, 28], where I_Q is the identity matrix. To construct the $Q \times (M - Q)$ matrix D , the algorithm randomly generates $M - Q$ bitstrings of length Q with the nearest even Hamming weight to the value $Q/2$, which we denote as $\text{even}(Q/2)$. Next, the algorithm censer a large set of flawed generators by check-

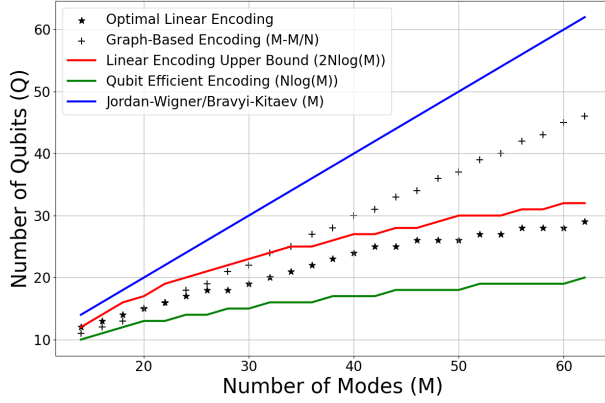


FIG. 1. This figure compares the qubit cost of the optimal linear encoding generated by RLE (star points) to the JW transformation (blue line), the current best linear encoding scheme in small M region – graph-based encoding (cross points), and QEE scheme (green line) for a 4 electron problem against the number of orbitals. We also compare the compression against the analytical upper bound in red.

Algorithm1 Randomized Linear Encoding

Input: Target States S ; Testing subset T_S ;
Output: Codeword C ;
while True **do**
 Initialized Codeword $C = []$;
 Random generate D with constraints;
 $G \leftarrow [I_Q | D]$;
 Create parity check matrix $P \leftarrow [-D^T | I_{M-Q}]$;
 Create a checking list $w = []$
 for t_s in T_S **do**
 $w \leftarrow [w | D_H(\sum P^T(t_s) \bmod 2, 0)]$
 end for
 if $\min(w) \geq 2N + 2$ **then**
 for s in S **do**
 $c = Gs$
 $C = [C | c]$
 end for
 if no repeat element in C **then**
 return C
 end if
 end if
end while

ing the Hamming weight of element \vec{k} generated by the $M - Q$ dimensional vector \vec{v} and the parity check matrix P :

$$\vec{k} = P\vec{v}, \vec{v} \in S \quad (8)$$

S is defined as the set of all vectors with Hamming weight 2 and $2K$ for $2K < N$, with K a randomly generated integer. Finally, we check whether the physical subspace is one-to-one encoded by explicitly computing the states. We repeat this process until we find the minimum Q . Preparing G in the standard form can reduce the randomized search. As we artificially increase the size of Q , RLE randomized search overhead will exponentially reduce and converge to a deterministic technique, see de-

tails in appendix F.

Numerical Test—We have analyzed the compression rate Q/M and presented the results in Table II. Our compression rate for linear encoding is better than previous works [10], *across all scenarios*. For instance, a 2-electron problem with 100 modes can be encoded with less than 20 qubits and a 4-electron problem with 400 modes in 50 qubits. Our numerical results all adhere to the $2N \log M$ logarithmic bound. For example, the numerical study in Figure 1 demonstrates that the optimal encoding lies within the $O(N \log M)$ scaling for a 4 electron problem.

$\begin{matrix} Q \\ N \backslash M \end{matrix}$	10	12	14	16	18	20	22	24	26	28	30
2	22	36	48	64	90	118	158	226	316	420	580
3	13	20	25	31	38	46	58	72	88	105	140
4	11	14	18	23	27	31	36	42	50	60	71
5	11	14	16	19	22	26	31	34	39	44	49
6	11	13	16	18	21	23	27	31	34	37	41

TABLE II. The numerical result of random compression. This table shows the maximum number of modes M that we can encode given the number of electron N (rows) and qubits Q (columns) with RLE. All results were computed on an 8-core laptop.

VQE Result—Here, we explore the performance of VQE for solving the compressed Hamiltonian of molecules using numerical simulations. Common approaches for solving molecular systems are to use the Hartree-Fock state as the initial state [29] and apply either hardware-efficient ansatz (HEA) [21, 22] or chemistry-inspired ansatz such as the Unitary Couple Cluster (UCC) ansatz [30–32]. With RLE, we can further compress the Hartree-Fock initial state. We choose to use HEAs as the ansatz because UCC-type ansatz has higher CNOT overhead as shown in Appendix F.

We benchmark the potential energy curves for the H_2 [33] molecule (2 electrons, 12 spin orbitals) against full configuration interactions (FCI). The errors are defined as the absolute difference between the estimated ground state energy and the FCI ground state energy. The calculation is performed in the 6-31G* basis and is compressed to 7 qubits. Figure 2 (a) shows that the HEA-RLE energies closely match the FCI curve for the H_2 potential energy. Figure 2 (b) shows the energy error of all points and the chemical accuracy threshold (1 Kcal/mol). At near equilibrium bond length of 0.75 Angstrom, the HEA-RLE ground state energy has error $\Delta E = |E - E_{FCI}| = 0.237$ Kcal/mol, which is within chemical accuracy.

Next, we investigate the performance of VQE on noisy quantum circuits. We use the HEA to solve a 2-electron LiH system [34] with 8 modes in both noise-free and noisy environments. For the noisy simulation, we use the Qiskit simulator with depolarizing errors of 10^{-3} and 10^{-4} on CNOT and single qubit gates, respectively. Table V shows the results for different HEA circuit depths. We find that the RLE Hamiltonian can achieve chemical

Models	LiH 6-31G (8 qubits)					LiH 6-31G (6 qubits)				
Repetitions	1	2	3	4	5	1	2	3	4	5
Number of Parameters	16	24	32	40	48	12	18	24	30	36
Number of CNOT	7	14	21	28	35	5	10	15	20	25
Noise Free Energy Error (kcal/mol)	2.49334	0.99961	0.56021	0.48336	0.41258	0.85701	0.40274	0.00333	0.00095	0.00002
Noisy Energy Error (kcal/mol)	2.49405	0.99942	2.14416	45.6810	92.1678	0.85701	0.54978	0.40319	1.40164	10.3847

TABLE III. This table compares the VQE result of 8-spin orbital 2-electron STO-3G LiH with the bond length 2.5 angstroms with and without compression. We study the the VQE noiseless and noisy energy error with respect to the hardware efficient circuit depth, and show that the compressed problem performs better in situation.

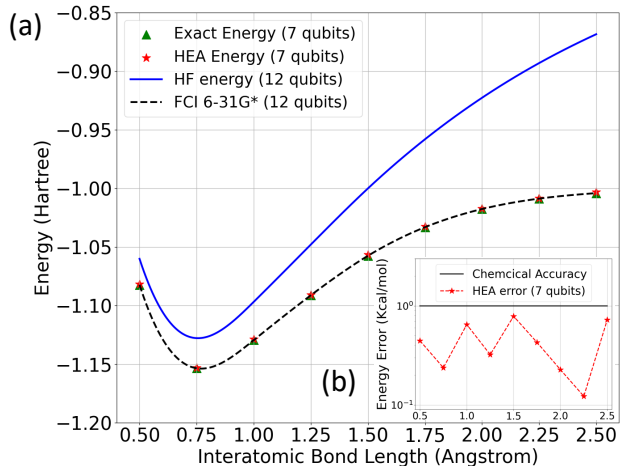


FIG. 2. Result of 12 modes 2 electrons 6-31G* H_2 potential energy curves encoded with 7 qubits. (a), the x-axis and y-axis respectively denote the Interatomic Bond Length in Angstrom, and energy in Hartree. (b), energy error plot with the y-axis in Kcal/mol.

accuracy for all circuit depths, while the JW Hamiltonian only barely achieves chemical accuracy at repetition 2.

A comparison of the HEA ansatz training result between the uncompressed and compressed Hilbert space shows that HEA performs substantially better in the compressed subspace, regardless of circuit depth or the presence of noise. We have also realised that linear compression can avoid barren plateaus contributed by the unphysical states. Further discussion is available in Appendix F. Thus, our result concludes that imposing conservation as a qubit cost constraint is an effective tool for comprehensively enhancing the expressivity, and trainability of a quantum circuit that is less susceptible to the damage of noise.

Conclusion – In this Letter, we have studied the art of linearly encoding particle-conserved electronic problems. We connect particle-conserved linear encoding to classical error correction via the parity check matrix – a new

protocol for constructing particle-conserved codes. The new protocol allows us to show that the optimal number-conserved linear compression has an upper bound of $2N \log_2 M$. We proposed a protocol for preparing efficient measurement bases for the 2-RDM. This protocol has indicated that the measurement complexity of linear encoding has an upper bound of $1 + \binom{M}{2} + \binom{M}{4}$, and the first and second excitations are exactly implementable in a linearly encoded space. However, optimal linear encoding also increases the gate complexity to $\mathcal{O}(M^N)$. These bounds imply that linear encoding should be preferred for encoding electronic structure Hamiltonian up to logarithmic qubit scaling.

In order to generate the optimal linear compression, we proposed a new algorithm. We have run a VQE experiment on the H_2 in 6-31G* against FCI with the optimal compression, and find that the results are within the chemical accuracy across all bond lengths. We have also compared the noisy and noiseless VQE experiment of LiH in STO-3G basis between the compressed and uncompressed problem with the hardware efficient ansatz at different circuit depths and showed VQE result is better across all situations. We have implemented the first optimal linear encoding for fermionic problems and have demonstrated advantages in implementing VQE problems due to the logarithmic qubit cost and polynomial measurement cost.

Finally, we observe a trade-off between linear compressed problems and gate complexity, but how to optimize between the two remains to be solved.

Acknowledgement – AH gratefully acknowledges the sponsorship from Research Grants Council of the Hong Kong Special Administrative Region, China (Project No. CityU 11200120), City University of Hong Kong (Project No. 7005615, 7006103), CityU Seed Fund in Micro-electronics (Project No. 9229135), and Hong Kong Institute for Advanced Study, City University of Hong Kong (Project No. 9360157). MSK thanks the Samsung GRC project and the UK EPSRC (EP/@032643/1 and EP/Y004752/1). This work was supported by the project AnQuC-3 of the Competence Center Quantum Computing Rhineland Palatinate (Germany).

- [2] Alexei Kitaev and Chris Laumann. Topological phases and quantum computation, 2009.
- [3] Christian W. Bauer, Zohreh Davoudi, A. Baha Balantekin, Tanmoy Bhattacharya, Marcela Carena, Wibe A. de Jong, Patrick Draper, Aida El-Khadra, Nate Gemelke, Masanori Hanada, Dmitri Kharzееv, Henry Lamm, Ying-Ying Li, Junyu Liu, Mikhail Lukin, Yannick Meurice, Christopher Monroe, Benjamin Nachman, Guido Pagano, John Preskill, Enrico Rinaldi, Alessandro Roggero, David I. Santiago, Martin J. Savage, Irfan Siddiqi, George Siopsis, David Van Zanten, Nathan Wiebe, Yukari Yamauchi, Kübra Yeter-Aydeniz, and Silvia Zorzetti. Quantum simulation for high energy physics, 2022.
- [4] Alan Ho, Jarrod McClean, and Shyue Ping Ong. The Promise and Challenges of Quantum Computing for Energy Storage. *Joule*, 2(5):810–813, May 2018.
- [5] Raffaele Santagati, Alan Aspuru-Guzik, Ryan Babbush, Matthias Degroote, Leticia Gonzalez, Elica Koyseva, Nikolaj Moll, Markus Oppel, Robert M. Parrish, Nicholas C. Rubin, Michael Streif, Christofer S. Tautermann, Horst Weiss, Nathan Wiebe, and Clemens Utschig-Utschig. Drug design on quantum computers, 2023.
- [6] J. Zhang, P. W. Hess, A. Kyprianidis, P. Becker, A. Lee, J. Smith, G. Pagano, I.-D. Potirniche, A. C. Potter, A. Vishwanath, N. Y. Yao, and C. Monroe. Observation of a discrete time crystal. *Nature*, 543(7644):217–220, mar 2017.
- [7] Richard P Feynman et al. Simulating physics with computers. *Int. j. Theor. phys*, 21(6/7), 2018.
- [8] Pascual Jordan and Eugene P. Wigner. About the Pauli exclusion principle. *Z. Phys.*, 47:631–651, 1928.
- [9] Mark Steudtner and Stephanie Wehner. Fermion-to-qubit mappings with varying resource requirements for quantum simulation. *New Journal of Physics*, 20(6):063010, jun 2018.
- [10] Sergey Bravyi, Jay M Gambetta, Antonio Mezzacapo, and Kristan Temme. Tapering off qubits to simulate fermionic hamiltonians. *arXiv preprint arXiv:1701.08213*, 2017.
- [11] William Kirby, Bryce Fuller, Charles Hadfield, and Antonio Mezzacapo. Second-quantized fermionic operators with polylogarithmic qubit and gate complexity. *PRX Quantum*, 3(2):020351, 2022.
- [12] Yu Shee, Pei-Kai Tsai, Cheng-Lin Hong, Hao-Chung Cheng, and Hsi-Sheng Goan. Qubit-efficient encoding scheme for quantum simulations of electronic structure. *Physical Review Research*, 4(2):023154, 2022.
- [13] William J. Huggins, Jarrod R. McClean, Nicholas C. Rubin, Zhang Jiang, Nathan Wiebe, K. Birgitta Whaley, and Ryan Babbush. Efficient and noise resilient measurements for quantum chemistry on near-term quantum computers. *npj Quantum Information*, 7(1):23, February 2021.
- [14] Jacob T Seeley, Martin J Richard, and Peter J Love. The bravyi-kitaev transformation for quantum computation of electronic structure. *The Journal of chemical physics*, 137(22):224109, 2012.
- [15] James J. Shepherd, Andreas Grüneis, George H. Booth, Georg Kresse, and Ali Alavi. Convergence of many-body wave-function expansions using a plane-wave basis: From homogeneous electron gas to solid state systems. *Physical Review B*, 86(3), jul 2012.
- [16] Andreas Grüneis, James J. Shepherd, Ali Alavi, David P. Tew, and George H. Booth. Explicitly correlated plane waves: Accelerating convergence in periodic wavefunction expansions. *The Journal of Chemical Physics*, 139(8):084112, 08 2013.
- [17] Kishor Bharti, Alba Cervera-Lierta, Thi Ha Kyaw, Tobias Haug, Sumner Alperin-Lea, Abhinav Anand, Matthias Degroote, Hermann Heimonen, Jakob S. Kottmann, Tim Menke, Wai-Keong Mok, Sukin Sim, Leong-Chuan Kwek, and Alán Aspuru-Guzik. Noisy intermediate-scale quantum algorithms. *Reviews of Modern Physics*, 94(1), feb 2022.
- [18] E. N. Gilbert. A comparison of signalling alphabets. *The Bell System Technical Journal*, 31(3):504–522, 1952.
- [19] R. R. Varshamov. Estimate of the number of signals in error correcting codes. *Dokl. Akad. Nauk SSSR*, 117:739–741, 1957.
- [20] Jules Tilly, Hongxiang Chen, Shuxiang Cao, Dario Piccozzi, Kanav Setia, Ying Li, Edward Grant, Leonard Wossnig, Ivan Rungger, George H. Booth, and Jonathan Tennyson. The variational quantum eigensolver: A review of methods and best practices. *Physics Reports*, 986:1–128, nov 2022.
- [21] Abhinav Kandala, Antonio Mezzacapo, Kristan Temme, Maika Takita, Markus Brink, Jerry M. Chow, and Jay M. Gambetta. Hardware-efficient variational quantum eigensolver for small molecules and quantum magnets. *Nature*, 549(7671):242–246, September 2017. Number: 7671 Publisher: Nature Publishing Group.
- [22] Xiongzi Zeng, Yi Fan, Jie Liu, Zhenyu Li, and Jinlong Yang. Quantum neural network inspired hardware adaptable ansatz for efficient quantum simulation of chemical systems, 2023.
- [23] R. Barends, L. Lamata, J. Kelly, L. García-Álvarez, A. G. Fowler, A. Megrant, E. Jeffrey, T. C. White, D. Sank, J. Y. Mutus, B. Campbell, Yu Chen, Z. Chen, B. Chiaro, A. Dunsworth, I.-C. Hoi, C. Neill, P. J. J. O’Malley, C. Quintana, P. Roushan, A. Vainsencher, J. Wenner, E. Solano, and John M. Martinis. Digital quantum simulation of fermionic models with a superconducting circuit. *Nature Communications*, 6(1):7654, July 2015. Number: 1 Publisher: Nature Publishing Group.
- [24] Yuan Su, Dominic W. Berry, Nathan Wiebe, Nicholas Rubin, and Ryan Babbush. Fault-tolerant quantum simulations of chemistry in first quantization. *PRX Quantum*, 2(4), nov 2021.
- [25] Ryan Babbush, Dominic W Berry, Yuval R Sanders, Ian D Kivlichan, Artur Scherer, Annie Y Wei, Peter J Love, and Alán Aspuru-Guzik. Exponentially more precise quantum simulation of fermions in the configuration interaction representation. *Quantum Science and Technology*, 3(1):015006, 2017.
- [26] Chee-Kong Lee, Chang-Yu Hsieh, Shengyu Zhang, and Liang Shi. Variational quantum simulation of chemical dynamics with quantum computers, 2021.
- [27] *Introduction to the Theory of Error-Correcting Codes*, chapter 1, pages 1–15. John Wiley /& Sons, Ltd, 1998.
- [28] *Introduction to the Theory of Error-Correcting Codes*, chapter 2, pages 17–38. John Wiley /& Sons, Ltd, 1998.
- [29] Google AI Quantum, Collaborators*†, Frank Arute, Kunal Arya, Ryan Babbush, Dave Bacon, Joseph C. Bardin, Rami Barends, Sergio Boixo, Michael Broughton, Bob B. Buckley, David A. Buell, Brian Burkett, Nicholas Bushnell, Yu Chen, Zijun Chen, Benjamin Chiaro,

Roberto Collins, William Courtney, Sean Demura, Andrew Dunsworth, Edward Farhi, Austin Fowler, Brooks Foxen, Craig Gidney, Marissa Giustina, Rob Graff, Steve Habegger, Matthew P. Harrigan, Alan Ho, Sabrina Hong, Trent Huang, William J. Huggins, Lev Ioffe, Sergei V. Isakov, Evan Jeffrey, Zhang Jiang, Cody Jones, Dvir Kafri, Kostyantyn Kechedzhi, Julian Kelly, Seon Kim, Paul V. Klimov, Alexander Korotkov, Fedor Kostritsa, David Landhuis, Pavel Laptev, Mike Lindmark, Erik Lucero, Orion Martin, John M. Martinis, Jarrod R. McClean, Matt McEwen, Anthony Megrant, Xiao Mi, Masoud Mohseni, Wojciech Mruczkiewicz, Josh Mutus, Ofer Naaman, Matthew Neeley, Charles Neill, Hartmut Neven, Murphy Yuezhen Niu, Thomas E. O'Brien, Eric Ostby, Andre Petukhov, Harald Putterman, Chris Quintana, Pedram Roushan, Nicholas C. Rubin, Daniel Sank, Kevin J. Satzinger, Vadim Smelyanskiy, Doug Strain, Kevin J. Sung, Marco Szalay, Tyler Y. Takeshita, Amit Vainsencher, Theodore White, Nathan Wiebe, Z. Jamie Yao, Ping Yeh, and Adam Zalcman. Hartree-fock on a superconducting qubit quantum computer. *Science*, 369(6507):1084–1089, 2020.

- [30] Joonho Lee, William J. Huggins, Martin Head-Gordon, and K. Birgitta Whaley. Generalized unitary coupled cluster wave functions for quantum computation. *Journal of Chemical Theory and Computation*, 15(1):311–324, nov 2018.
- [31] Jonathan Romero, Ryan Babbush, Jarrod R. McClean, Cornelius Hempel, Peter Love, and Alán Aspuru-Guzik. Strategies for quantum computing molecular energies using the unitary coupled cluster ansatz, 2018.
- [32] Yangchao Shen, Xiang Zhang, Shuaining Zhang, Jing-Ning Zhang, Man-Hong Yung, and Kihwan Kim. Quantum implementation of the unitary coupled cluster for simulating molecular electronic structure. *Physical Review A*, 95(2), feb 2017.
- [33] Jiangfeng Du, Nanyang Xu, Xinhua Peng, Pengfei Wang, Sanfeng Wu, and Dawei Lu. Nmr implementation of a molecular hydrogen quantum simulation with adiabatic state preparation. *Phys. Rev. Lett.*, 104:030502, Jan 2010.
- [34] Julia E. Rice, Tanvi P. Gujarati, Mario Motta, Tyler Y. Takeshita, Eunseok Lee, Joseph A. Latone, and Jeanette M. Garcia. Quantum computation of dominant products in lithium–sulfur batteries. *The Journal of Chemical Physics*, 154(13):134115, apr 2021.
- [35] Single and double excitation corresponds to Pauli-X operator with Pauli weight 4, which is why $N \geq 4$ will allow for distinct single and double excitation encoding.
- [36] F. J. MacWilliams and N. J. A. Sloane. *The Theory of Error Correcting Codes*. North-Holland Pub. Co., 1977.
- [37] Fernando Hernando, Francisco D. Igual, and Gregorio Quintana-Ortí. Algorithm 994: Fast implementations of the brouwer-zimmermann algorithm for the computation of the minimum distance of a random linear code. *ACM Trans. Math. Softw.*, 45(2), jun 2019.
- [38] Igor O Sokolov, Panagiotis Kl Barkoutsos, Pauline J Ollitrault, Donny Greenberg, Julia Rice, Marco Pistoia, and Ivano Tavernelli. Quantum orbital-optimized unitary coupled cluster methods in the strongly correlated regime: Can quantum algorithms outperform their classical equivalents? *The Journal of chemical physics*, 152(12), 2020.

Appendix A: Framework for number-conserved Linear Encoding

We provide a detailed discussion of the dual code correspondence that connects number-conserved linear encoding classical error correcting code, inspired from previous work [10]. The insight lies in the observation that constraining the dual code of \mathbf{G} is the same as constraining the code \mathbf{P} itself.

We can think of \mathbf{P} as generating equivalent class C on the M dimensional binary vector space \mathbb{F}_2^M :

$$C = \{\vec{v} \in \mathbb{F}_2^M, \forall \vec{c} \in \mathbb{F}_2^{M-Q} | \vec{v} = \mathbf{P}^T \vec{c}\} \quad (\text{A1})$$

This class C is mapped to the zero codeword in the encoded space and defines the equivalent class with other bitstrings $\vec{b} \in \mathbb{F}_2^M$ via the following action:

$$\vec{b} \rightarrow \vec{b} \oplus C \quad (\text{A2})$$

$\vec{b} \oplus C$ is a left coset that is isomorphic to the space generated by \mathbf{G} . The conserved quantity N then imposes a constraint on the coset such that each bitstring with Hamming weight N shall only appear once in this coset. This constraint then becomes a constraint on the Hamming weight of \mathbf{P} . If \mathbf{P} generates even subspace with code distance $2N + 2$, then for the subspace with Hamming weight less than or equal to N , \mathbf{G} will distinctively encode them into the encoded space. Proof of this statement is available in Lemma 1. That is, we can generate arbitrary odd equivalent classes because they do not contribute to mapping bitstrings with the same parity.

As we will show in the proof of Theorem 1, that is equivalent to saying that we would like our \mathbf{P} to have one unconstrained row element with odd Hamming weight. As for the rest of the row, it is a code with even Hamming weight and distance $2N + 2$. Thus, we now need only to find error correcting code of dimension $(M - Q - 1) \times M$ with even Hamming weight and distance $2N + 2$ for us to construct a valid $Q \times M$ number-conserved linear encoding. The code is characterised by the parameter $[M, M - Q - 1, 2N + 2]$.

Appendix B: Framework for Qubit Operator Encoding

Here, we discuss our qubit operator encoding framework using linear space. In this framework, we can efficiently encode the qubit operator with binary vector compression.

First, we introduce the encoding of the projector. Literature such as Ref~[12] and [26] employ projectors for approaching the $[N \log_2 M]$ lower bound. However, both methods suffer from unscalable measurement costs. One reason behind this broken scaling is due to the breaking of the linear structures of the projectors. In our framework, we connect the projector to linear binary vector

space, which allows us to assess the measurement complexity with the linear structure.

1. Encoding projectors

Definition 1. *Projectors in the computational basis are defined as:*

$$P^0 = |0\rangle\langle 0| = \frac{1+Z}{2} \quad (B1)$$

$$P^1 = |1\rangle\langle 1| = \frac{1-Z}{2} \quad (B2)$$

which satisfies the following properties:

$$P^0 P^1 = 0 \quad (B3)$$

$$P^a P^a = P^a \text{ for } a \in \{0, 1\} \quad (B4)$$

$$I_2 = P^0 + P^1. \quad (B5)$$

Definition 2. *Tensor products of projectors are defined as:*

$$P^{\vec{a}} = \prod_{m=1}^M P_m^{\vec{a}[m]} \quad (B6)$$

with $\vec{a}[m]$ denotes the m th entry of the binary vector, and P_m denotes projector on the m th qubit. As an example, if we would like to project to a specific bitstring $|0011\rangle$, then:

$$P^{0011} |0011\rangle = |0011\rangle \quad (B7)$$

$$P^{0011} |1010\rangle = 0. \quad (B8)$$

2. Encoding Pauli-X and Z operators

Definition 3. *Let $\vec{b} \in \mathbb{F}_2^M$ be a binary vector, we defined what we called an X-string as follows:*

$$X^{\vec{b}} = \prod_{m=1}^M X_m^{\vec{b}[m]} \quad (B9)$$

with $\vec{b}[m]$ denotes the m th entry of the vector.

The action of $X^{\vec{b}}$ on a bitstring state vector \vec{a} can be understood as:

$$X^{\vec{b}} |a\rangle = |\vec{a} \oplus \vec{b}\rangle \quad (B10)$$

Definition 4. *Let $\vec{b} \in \mathbb{F}_2^M$ be a binary vector, we define a Z-string as follows:*

$$Z^{\vec{b}} = \prod_{m=1}^M Z_m^{\vec{b}[m]} \quad (B11)$$

The action of $Z^{\vec{b}}$ on a bitstring state vector \vec{a} becomes:

$$\langle \vec{a} | Z^{\vec{b}} | \vec{a} \rangle = (-1)^{\vec{b} \cdot \vec{a}} \quad (B12)$$

Let's define $\vec{s}_i \in \mathbb{F}_2^M$ be the set of vectors with Hamming weight 1. From Eqn~(B10), we can immediately infer that the encoding of a Pauli-X operator transforms under bitwise linear encoding as:

$$\mathcal{E}(X_i) = \prod_{m=1}^Q X_m^{\mathbf{G}\vec{s}_i[m]} \quad (B13)$$

with \mathbf{G} the encoding matrix. From this relation, we know that the encoding of Pauli-X operator is *the same* as the encoding of bitstring [35]. With linearity, we can then trivially encode the tensor product of Pauli-X operators.

Suppose now we have a set of encoded bitstrings $\vec{a}_i = \mathbf{G}_i^j \vec{s}_j$, we can find a set of dual vectors $\vec{b}^j = \vec{s}^j (\mathbf{G}^{-1})_i^j$ such that:

$$\vec{b}^j \cdot \vec{a}_i = \delta_i^j. \quad (B14)$$

The orthogonality ensures that each encoded Pauli-Z operator only detects a negative sign on the bitstring $\mathbf{G}_i^j \vec{s}_j$. In the scope of qubit operator transformation, this is equivalent to ensuring that the exponent of Eqn~(B12) satisfies Eqn~(B14). Thus, we infer that the encoding of the Pauli-Z operator transforms as:

$$\mathcal{E}(Z_i) = \prod_{m=1}^M Z_m^{(\mathbf{G}^{-1})^T \vec{s}_i[m]} \quad (B15)$$

Linear compression preserves Eqn~(B13), but breaks Eqn~(B15) due to the lack of left inverse of \mathbf{G} . Instead, the Pauli-Z operator is encoded as:

$$\mathcal{E}(Z_i) = 1 - 2 \sum_{\vec{a} \in S_{Z_i}} P^{\vec{a}} \quad (B16)$$

with $P^{\vec{a}}$ a Q qubits projector with convention defined in Definition 2. S_{Z_i} is the set of physical states that output a negative sign under the action of Z_i . This overhead would then contribute to extra gate complexity, and the sum over projector is related to parity check matrix \mathbf{P} .

With this framework, we can now derive a general representation of the qubit operator. In essence, all qubit operators consist of a selected set of states and transitions. In the computational basis, the X-string captures the transition, and the sum over projectors captures the states.

Provided with a X-strings $X^{\vec{a}}$ and a projector $P^{\vec{b}}$, we can observe the following property:

$$X^{\vec{a}} P^{\vec{b}} = P^{\vec{a} \oplus \vec{b}} X^{\vec{a}} \quad (B17)$$

we can represent the Hermitian or anti-Hermitian part of the operator as:

$$(X^{\vec{a}} (P^{\vec{b}} \pm P^{\vec{a} \oplus \vec{b}}))^{\dagger} = \pm X^{\vec{a}} (P^{\vec{b}} \pm P^{\vec{a} \oplus \vec{b}}). \quad (B18)$$

Summation over this basis operator with respect to the Boolean vector \vec{a} and \vec{b} will allow us to construct arbitrary (anti-)Hermitian qubit operators. As we will show in Theorem 2, one X-string with an arbitrary sum over projector $P^{\vec{b}}$ and its conjugate $P^{\vec{a} \oplus \vec{b}}$ generates commuting Pauli strings as we expand the projector. Thus, the number of X-strings in fact determines the measurement cost of a given qubit operator. Suppose now we exponentiate the Hermitian operator. The number of X-strings then determines how many trotterisation steps are required to approximate the unitary evolution.

In the JW representation, the product of creation and annihilation operators always corresponds to one X-string. Linear encoding would then surjectively encode the JW X-strings. This property allows us to exactly implement fermionic gates and efficiently prepare measurement bases for fermionic observables.

Appendix C: Qubit Complexity Proof

Lemma 1. *Given bitwise linear map \mathcal{E} which is number-conserved, for all bitstrings k which is an element of $\ker \mathcal{E}$, $D_H(k, 0) \geq 2N + 2$ if $D_H(k, 0) \equiv 0 \pmod{2}$.*

Proof. First, the theorem is equivalent to stating that the even Hamming weight codewords, generated from the parity check matrix \mathbf{P} , must be lower bounded by $2N + 2$.

Now, suppose that there is a bitstring \vec{k} with Hamming weight $2K < 2N + 2$, then we construct two distinct bitstrings with Hamming weight N such that $\vec{d} = \vec{c} \oplus \vec{k}$. Under this construction, the \vec{c} and \vec{d} has $N - K$ overlapping bits. We observe the following relation in the encoded space

$$\mathcal{E}(\vec{d}) = \mathcal{E}(\vec{c}) \oplus \mathcal{E}(\vec{k}) = \mathcal{E}(\vec{c}). \quad (\text{C1})$$

□

Theorem 1. *The minimal qubit cost required to encode a M fermionic modes N electrons problem has the upper bound of $Q \leq 2N \log M$.*

Proof. From Theorem 1, we observe that all even kernel elements k , generated by the Parity check matrix \mathbf{P}^T , have even Hamming weight lower bounded as $D_H(k, 0) \geq 2N + 2$. We can interpret the row of the parity check matrix \mathbf{P} as a $M - Q$ set of M -bit bitstrings, whose arbitrary bitwise addition \oplus among the bitstrings are encoded into the $\mathbf{0}$ vector in the encoded space. Since \mathbf{P} is invariant under elementary bitwise row addition, it is possible to eliminate the odd Hamming weight M -bit bitstrings with odd Hamming weight M -bit bitstrings. \mathbf{P} can be reorganized as a set of M -bit bitstrings with *only one* element with odd Hamming weight. In this form, we can impose Theorem 1 on the $M - Q - 1$ numbers of M -bit bitstrings.

Next, we reformulate the constraint as finding the maximal $M - Q - 1$ of \mathbf{P} given qubits M , and minimal hamming distance $2N + 2$, and all Hamming weight of elements in

\mathbf{P} are even. Borrowing from classical error correction, the maximum is upper bounded by the Hamming bound [36] and lower bounded by the Gilbert–Varshamov bound [18, 19].

$$\frac{2^{M-1}}{\sum_{j=0}^N \binom{M}{2j}} \leq 2^{M-Q-1} < \frac{2^{M-1}}{\sum_{j=0}^{\lfloor \frac{N}{2} \rfloor} \binom{M}{2j}} \quad (\text{C2})$$

$$\begin{aligned} M - 1 - \log_2 \sum_{j=0}^N \binom{M}{2j} &\leq M - Q - 1 \\ &< M - 1 - \log_2 \sum_{j=0}^{\lfloor N/2 \rfloor} \binom{M}{2j} \\ 2N \log_2 M &\geq Q > 2 \left\lfloor \frac{N}{2} \right\rfloor \log_2 M. \end{aligned} \quad (\text{C3})$$

We modify the Hamming and Gilbert–Varshamov bound in Eqn~(C2) such that we are only considering the bound on the even Hamming weight subspace, which has size 2^{M-1} ; and the sum $\sum_{j=0}^N \binom{M}{2j}$ is only over the even binomial coefficients. However, the argument of the Hamming cube as the maximal non-overlapping covering remained unchanged [18]. We also note that the Hamming bound for even subspace becomes a strict non-equality because the covering space does not cover the whole even code subspace.

We have proved that optimal bitwise linear encoding has $\mathcal{O}(N \log M)$ scaling. In particular, the lower bound coincides with the scaling of physical states. □

Appendix D: Proof for Measurement Complexity

Lemma 2. *All fermionic operators that can be written as a product of creation and annihilation operators can be expressed in terms of the product of one X-string and sum over P-strings under linear compression.*

Proof. First, we consider the Jordan–Wigner basis. The one particle creation and annihilation operators are written as the product of the Pauli-Z operator Z_m , Pauli-X operator X_i , and projector $P_i^{0/1}$ defined in Def. B2:

$$\hat{a}_i^\dagger = \prod_{m=1}^{i-1} Z_m X_i P_i^0 \quad (\text{D1})$$

$$\hat{a}_j = \prod_{m=1}^{j-1} Z_m X_j P_j^1. \quad (\text{D2})$$

Next, we observe that for each qubit i , $P_i^{0/1}$ represents the set of bitstrings such its entry in the i th qubit is 0/1. Thus, it is possible to expand $P_i^{0/1}$ as a sum over projector strings $P^{a_1 a_2 \dots a_{M-1}}$ defined in Def. 2:

$$P_i^{0/1} = P_i^{0/1} \otimes \sum_{\vec{a} \in \{0,1\}^{M-1}} P^{\vec{a}}. \quad (\text{D3})$$

Thus, the Z-strings, $\prod_{m=1}^{i-1} Z_m$ from the above example, can be absorbed into the projectors via the relationship:

$$Z^{\vec{c}} P^{\vec{b}} = (-1)^{\vec{c} \cdot \vec{b}} P^{\vec{b}}. \quad (\text{D4})$$

After this procedure, we need only the X-strings, projectors, and signs with respect to the projectors to encode a fermionic gate. Since each projector represents a fermionic state, we need to discard the unphysical states such that the encoded projectors would not coincide with the number-conserved projectors. Let us denote \hat{O} as the product of creation and annihilation operators. Given a linear encoder $\mathcal{E}(\cdot)$ we can succinctly express the unencoded and encoded gates as follows:

$$\hat{O} = X^{\vec{a}} \sum_{\vec{b} \in S_{\hat{O}}} (-1)^{\vec{c} \cdot \vec{b}} P^{\vec{b}} \quad (\text{D5})$$

$$\mathcal{E}(\hat{O}) = X^{\vec{G}\vec{a}} \sum_{\vec{b} \in S_{\hat{O}}} (-1)^{\vec{c} \cdot \vec{b}} P^{\vec{G}\vec{b}} \quad (\text{D6})$$

where $S_{\hat{O}}$ represents the set of number-conserved states on which \hat{O} acts, and $\vec{a}, \vec{c} \in \mathbb{F}_2^M$ are binary vector uniquely associated with each operator \hat{O} , and \vec{a} induces physical state transition and \vec{c} encodes the sign information for each vector \vec{b} . \square

Lemma 3. *The real and imaginary part of an observable $\text{Re/Im}\{\hat{O}\}$, provided that it can be written as a product of one X-string and a sum over pair of conjugate projectors defined in Eqn~(B18), can be measured with one measurement basis under linear encoding.*

Proof. From Eqn~(B18) and Eqn~(D6), We can write the (anti-)Hermitian part of the operators as:

$$\text{Re/Im}\{\mathcal{E}(\hat{O})\} = X^{\vec{G}\vec{a}} \sum_{\vec{b} \in S_{\hat{O}}} (-1)^{\vec{c} \cdot \vec{b}} (P^{\vec{G}\vec{b}} \pm P^{\vec{G}(\vec{a} \oplus \vec{b})}). \quad (\text{D7})$$

We make use of the following CNOT transformation to eliminate the extra Pauli-X operations:

$$\text{CNOT}_{1,2} X_1 X_2 \text{CNOT}_{1,2} = X_1 \quad (\text{D8})$$

$$\text{CNOT}_{1,2} P^{a_1 a_2} \text{CNOT}_{1,2} = P^{a_1(a_1 \oplus a_2)} \quad (\text{D9})$$

where we define i as control qubit and j as target qubit for $\text{CNOT}_{i,j}$. Applying the Eqn~(D9) on a pair of conjugate projectors in the form of Eqn~(B18), we observe that the projector pair at the target qubit will become the same. Inductively eliminating the Pauli-X operator with CNOT on the sum of pairs in Eqn~(D7), we are left with the last qubit that has one Pauli-X/Y operator to act on, and a sum over projectors at the other qubits:

$$\hat{C} \text{Re/Im}\{\mathcal{E}(\hat{O})\} \hat{C}^\dagger = \sum_{\vec{m}} X_N (P_N^0 P^{\vec{m}} \pm P_N^1 P^{\vec{m}}) \quad (\text{D10})$$

where \hat{C} denotes the overall Clifford transformation, \vec{m} is a $Q-1$ dimensional vector belonged to $S_{\hat{O}}$ set under the

Clifford transformation, X_N denotes the Pauli-X operator acting on the N th qubit, and similarly for $P_N^{0/1}$. On qubit N , the sum of P^0 and P^1 generates local I or difference generates Z_N . We can rewrite them as X_N or $-iY_N$.

Since all operators, except the qubit Q which is either X_i when hermitian or iY_Q otherwise, are projectors made of I, Z operators, the real/imaginary part of the bitwise linear encoded operators must generate commuting Pauli string in the Clifford transformed basis. Finally, since Clifford transforms one-to-one encoded Pauli strings, the operator $\text{Re/Im}\{\mathcal{E}(\hat{O})\}$ also generates commuting Pauli strings. \square

Theorem 2. *The cost of measurement basis of a linearly encoded quantum chemistry Hamiltonian is upper bounded by $1 + \binom{M}{2} + \binom{M}{4}$.*

Proof. First, we observe that the 2-RDM are the physical observables required to compute quantum chemistry properties, so we only need to determine the measurement complexity of 2-RDM.

Next, from Lemma 2 and 3, we see that the (anti-)Hermitian part of the 2-RDM, defined as $\langle \psi | \hat{a}_i^\dagger \hat{a}_j^\dagger \hat{a}_k \hat{a}_l \pm \hat{a}_l^\dagger \hat{a}_k^\dagger \hat{a}_j \hat{a}_i | \psi \rangle$, can be measured in one basis for each set of fermionic modes i, j, k, l . In quantum chemistry, we are only interested in the real part of the observables. Therefore, each i, j, k, l demands one measurement basis.

Due to the result in Lemma 3, each distinct X-string corresponds to one unique measurement basis. Upon encoding the 2-RDM operator via the JW transformation, we see that the encoded operator is of the form of the real part of Eqn~D5. The X-string in this JW representation is invariant under any permutation among i, j, k, l in the JW representation. Thus, the measurement scaling is equal to the possible combinations of i, j, k, l , where we allow the indices to be equal to each other. Next, we count the number of distinct X-strings derived from the possible permutation. In the JW representation, we can show that when all indices are not equal to each other, the number of distinct X-strings corresponds to the complete set of M dimensional binary vectors with Hamming weight 4. Meanwhile, when one pair of indices share the same digit, it corresponds to the set of M dimensional binary vectors with Hamming weight 2. When two pairs are equal, then it corresponds to M dimensional binary vectors with Hamming weight 0. Under our formalism, each X-string can be associated with a binary vector. Thus, the total measurement cost, without parallelization [13], is equal to $\binom{M}{0} + \binom{M}{2} + \binom{M}{4}$. We define parallelization to be a simultaneous measurement of two or more sets of RDM elements with indices, for example, i, j, k, l and m, n, o, p , such that there is no index overlap among the sets. Such parallelization would be destroyed under linear compression.

Finally, since a linear compression surjectively encodes the X-string guaranteed by the $2N+2$ code distance of the Parity check matrix \mathbf{P} , $\binom{M}{0} + \binom{M}{2} + \binom{M}{4}$ is the upper bound of the measurement scaling for the encoded space. \square

Corollary 1. *The scaling of measurement basis can be completely characterised by the number of distinct X-strings that appears in the X and P decomposition.*

Proof. From the previous proof, we observe the fact that each unique X-string, obtained from the X P decomposition of an operator, generates commuting Pauli strings. We can then also observe that Pauli strings generated by two distinct X-strings, and two pairs of respective projectors, contain mutually non-commuting terms. \square

This result can also be employed to characterize non-linear encoding, which *does not* surjectively encode X strings to X strings. Under non-linear encoding, Eqn~(D7) will further split into a sum over X strings. The characterization of scalable measurement then demands that the number of distinct X strings used to represent a Hamiltonian problem must be polynomially bounded, such that the measurement cost is polynomially lower bound.

Appendix E: Quantum Gate Encoding

Under the same framework, we show that linear encoding can exactly implement single and double excitation, a feature impossible for any non-linear encoding. However, we find ourselves with the following gate complexity.

Proposition 1. *Single and double excitations can be decomposed as a series of multi-control gates and CNOT gates.*

Proof. From Theorem 3, we can transform operators in Eqn~D7 into X-string with the Clifford transformation \hat{C} and operator of the form:

$$\hat{C} \text{Re/Im}\{\mathcal{E}(\hat{O})\}\hat{C}^\dagger = \sum_{\vec{m}} X_N / -iY_N P^{\vec{m}} \quad (\text{E1})$$

where $X_N / -iY_N$ is the last Pauli-X/Y operator at qubit N , which depends on the choice of the Clifford transform. Each operator $X_N / -iY_N P^{\vec{m}}$ then corresponds to a multi-control X/Y rotation, where the location of the projectors are the control bits. Meanwhile, \hat{C} is just a sequence of CNOT gate transformations. \square

The multi-control gates all commute with each other. Thus, we have also shown that the encoded fermionic single and double excitations do not require trotterization. Next, we can trivially show that the worst-case scenario gate complexity has combinatoric scaling, namely $\mathcal{O}(M^N)$. Given an operator \hat{O} , and the set of physical states it acts on $S_{\hat{O}}$, the number of multi-control gates is equal to the size of $S_{\hat{O}}$, which scales combinatorically. This leads to an open question of methods to eliminate the multi-control gates.

Appendix F: Numerical Details

1. Scaling of RLE

We examine the scalability of RLE. The algorithm has computation cost proportional to $\mathcal{O}(M^N)$ for each physical state check, times the number of times for checking; it has the same complexity scaling compared to the Brouwer-Zimmermann algorithm, the most efficient method for checking the minimal distance of \mathbf{P} [37]. RLE also has the identical computational cost as non-linear encoding [12], but it is much more straightforward to implement. We can further improve RLE scalability by adding auxiliary qubits to the optimal encoding. Figure 3 summarizes the success probability of generating the correct \mathbf{G} for 4-electron systems with auxiliary qubits. The algorithm runtime exponentially converges to $\mathcal{O}(M^N)$ – the complexity for one check – when successively adding the auxiliary qubits.

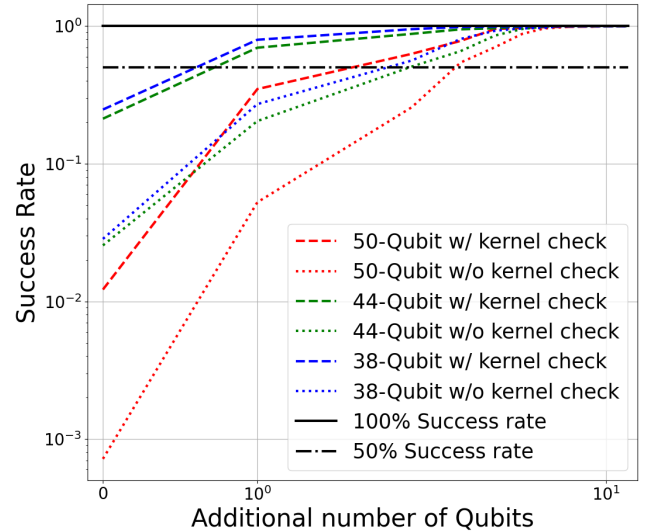
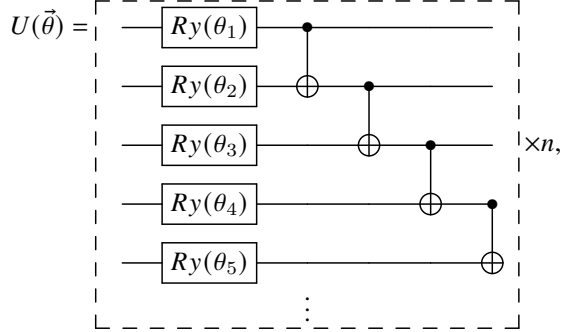


FIG. 3. This figure illustrates the impact on the success probability of generating \mathbf{G} when adding extra qubits to the generator. The x-axis shows the number of auxiliary qubits and the y-axis is the success rate. The dashed line, which resulted from a codeword check generated in Eqn~(8), shows a systematic improvement in success rate compared to the unchecked (dotted line) case.

a. Hardware-Efficient Ansatz

Hardware-efficient ansatz(HEA) is commonly used in VQE due to its resource efficiency against the noisy constraints of the current quantum devices. Different hardware have their own Hardware-Efficient setting including the use of the gates, circuit connectivity, and noise model. To fit the above criteria, here we design our HEA with two constraints. First, the gates we use for our VQE

simulations are restricted to the two qubits Controlled NOT gate and single qubit rotation Y gate. Second, the connectivity of the two-qubit gates is restricted on a 1D chain topology. The design of the ansatz is therefore as follows design,



the n is the number of repetitions of the circuit block.

b. Elementary Generator Matrix

The row-switching of the standard form generator matrix \mathbf{G} will be another valid generator matrix \mathbf{G}' . From the numerical test, we find out that encoding the fermionic Hamiltonian with \mathbf{G} and \mathbf{G}' will result in different convergence performances. An intuition to this phenomenon is that the expressibility will be limited using the fixed connectivity Hardware Efficient Ansatz, and a good initial state obtained from row-switching will improve the convergence. As shown in Figure 4, the different generator matrices will map the ground state in different state representations.

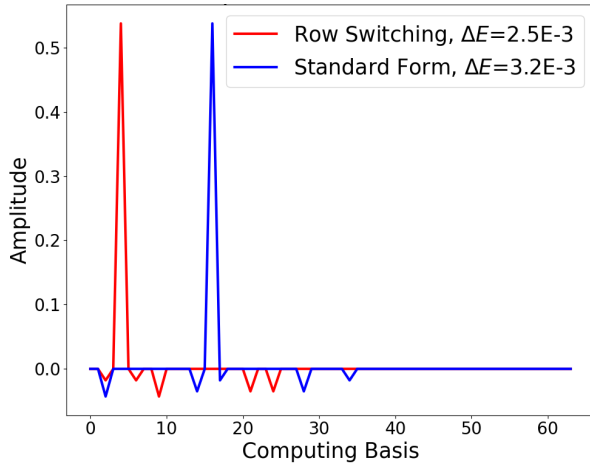


FIG. 4. The 6-qubit ground state of (8,2) LiH Hamiltonian. The x-axis is the computing basis and the y-axis is the amplitude. The row-switching generator matrix will have lower energy than the standard form generator matrix.

The above result indicates a possibility to optimize the encoding ansatz rather than optimize the circuit. In

practice, we can prepare the row-switching compressed Hamiltonians and use one or a few layers of the circuit to compare the convergence. The one with the lowest energy under the fixed connectivity shallow circuit will be used for deeper ansatz with the same connectivity for finding the ground state.

c. Compared with Unitary Couple Cluster type of Ansatz

We compared the performance of HEA ansatz in the compressed space to the UCC-type Ansatz [38], the golden standard to computational chemistry simulation, on ground state simulation of LiH in the STO-3G and 6-31G* basis. With the active space chosen as $M = 8$ and $M = 16$ fermionic modes respectively, we can restrict the Hilbert space generated from both bases to the two electrons subspace – denoted as (8,2) and (16, 2). In the STO-3G solution, both the 6-qubit compressed and 8-qubit uncompressed Hamiltonian can reach a chemical accuracy of 1 Kcal/mol using HEA with decent circuit depth. However, the 6-qubit Hamiltonian is 4 orders of magnitude more accurate compared to the 8-qubit Hamiltonian with less number of parameters and circuit depth. On the other hand, compared to HEA, the UCC-type ansatz converges faster and easier due to the small number of parameters, only at the expense of approximately 2-orders of magnitude deeper circuit and one order of magnitude the number of two-qubit gates to reach one order of magnitude higher accuracy of HEA results.

Systems	LiH (8,2)			
	HEA		UCC	
Ansatz Types	8 qubits	6 qubits	SUCCD	UCCSD
Number of Parameters	48	36	6	15
Number of CNOT	35	25	480	768
Circuit Depth	41	31	668	1043
ΔE (kcal/mol)	0.4126	0.0002	0.5216	0.00003

TABLE IV. This table showcases the noiseless simulation of (8,2) LiH using HEA and UCC-type ansatz. ΔE is the difference between the VQE energy and energy from exact diagonalisation. The HEA results are chosen from the lowest energy results using the VQE with L-BFGS-B optimizer and 100 different initial states. The UCCSD and SUCCD ansatz is constructed from Qiskit package

However, when the system scales up to (16,2) LiH, HEA on the uncompressed Hilbert space starts showing Barren Plateaus. The L-BFGS-B with 100 initial states does not converge to the required chemical accuracy. With the RLE, which encodes the original 16-qubit Hamiltonian with an 8-qubit Hamiltonian, HEA can converge to chemical accuracy. In conclusion, the LiH system scaling result shows that the qubit compression can improve VQE convergence while reducing the qubit cost and circuit depth. It can also mitigate HEA's Barren Plateaus problem when the system scales up with respect to the fermionic modes.

Systems	LiH (16,2)			
Ansatz Types	HEA		UCC	
	16 qubits	8 qubits	SUCCD	UCCSD
Number of Parameters	96	48	28	63
Number of CNOT	75	35	4032	7280
Circuit Depth	81	41	4874	8675
ΔE (kcal/mol)	2.2099	0.7186	0.5749	0.00001

TABLE V. This table showcases the noiseless simulation of (8,2) LiH using HEA and UCC-type ansatz. ΔE is the difference between the VQE energy and energy from exact diagonalisation. The HEA results are chosen from the lowest energy results using the VQE with L-BFGS-B optimizer and 100 different initial states. The UCCSD and SUCCD ansatz are constructed from the Qiskit package.